Photophysical, Dynamic and Redox Behavior of *tris*-(2,6-Diisopropylphenyl)phosphine

René T. Boeré,[1] Alan M. Bond,[2] Steve Cronin,[1] Noel W. Duffy,[2] Paul Hazendonk,[1] Jason D. Masuda,[1] Kyle Pollard,[1] Tracey L. Roemmele,[1] Peter Tran,[1] Yuankui Zhang,[1]*

Department of Chemistry and Biochemistry, The University of Lethbridge, Lethbridge, AB Canada T1K 3M4 and the School of Chemistry, Monash University, Clayton, Victoria 3800, Australia

Electronic Supplementary Information

[1] University of Lethbridge (boere@uleth.ca; +1-403-329-2045; Fax +1-403-329-2057

boere@uleth.ca

[2] Monash University (Alan.Bond@sci.monash.edu.au; +61 3 9905 1338; Fax +61 3 9905 4597)

Table S1. Interatomic distances [Å] and angles [°] for $Dipp_3P$ and $Dipp_3P^{+\bullet}$ from X-ray and Computation[1]

Dimension	Experiment C_3 $Dipp_3P$	C_3 in B3LYP/6-31G(d)	D_3 in B3LYP/6-31G(d)	C_3 in HF6/6-31G(d)	$[Dipp_3P]^+$ in UHF6/6-31G(d)
P-C1	1.8507(16)	1.8781	1.8142	1.8777	1.8353
C1-C6	1.418(2)	1.4236	1.4272	1.4122	1.4164
C1-C2	1.425(2)	1.4310		1.4221	1.4187
C2-C3	1.388(3)	1.3988	1.3980	1.3877	1.3964
C2-C7	1.517(3)	1.5348	1.5236	1.5354	1.5301
C3-C4	1.395(3)	1.3901	1.3945	1.3793	1.3843
C4-C5	1.368(4)	1.3869		1.3748	1.3852
C5-C6	1.403(3)	1.4034		1.3936	1.3962
C6-C10	1.514(3)	1.5291		1.5288	1.5273
C7-C9	1.531(3)	1.5412	1.5362	1.5354	1.5373
C7-C8	1.531(3)	1.5410	1.5451	1.5373	1.5362
C10-C12	1.529(3)	1.5405		1.5352	1.5365
C10-C11	1.531(3)	1.5441		1.5396	1.5378
P oop of C1 × 3 [2]	0.539	0.536	0	0.531	0.193
P oop C2-C3-C5-C6 [3]	0.430	0.434	0	0.424	0.060
C1#1-P-C1	111.88(5)	112.2	120.0	112.3	118.9
C6-C1-C2	118.90(16)	118.8	121.4	118.5	121.3
C6-C1-P	127.17(13)	126.8		127.2	122.5
C2-C1-P	113.10(12)	113.4	119.29	113.4	116.2
C3-C2-C1	119.67(17)	119.5	117.8	119.6	117.9
C3-C2-C7	117.58(17)	116.8	124.5	116.3	117.2
C1-C2-C7	122.75(15)	123.7	121.4	124.1	124.9
C2-C3-C4	121.0(2)	121.5	120.1	121.5	121.4
C5-C4-C3	119.51(19)	119.1		119.2	120.0
C4-C5-C6	122.0(2)	121.9		121.8	121.6
C5-C6-C1	118.8(2)	119.1		119.3	117.7
C5-C6-C10	117.42(19)	116.2		115.7	117.4
C1-C6-C10	123.75(17)	124.7		124.9	124.8
C2-C7-C9	110.48(18)	110.8	112.6	111.0	112.0
C2-C7-C8	111.87(19)	113.1	111.8	113.1	111.8
C9-C7-C8	110.9(2)	110.5	110.8	110.3	110.7
C6-C10-C12	112.4(2)	112.6		112.6	111.6
C6-C10-C11	111.2(2)	111.6		111.7	112.3
C12-C10-C11	109.9(2)	109.8		109.5	110.2

[1] Symmetry transformation used to generate equivalent atoms: #1 -x+y-1,-x-1,z. Atom numbering scheme, see following page.
[2] Plane of the three *ispo* C atoms of the aryl rings.
[3] Plane of the four *ortho* and *meta* C atoms of the aryl ring.

Table S2. Table of electronic spectra of $Dipp_3P$, $Dipp_3P^{+\bullet}$ and Ph_3P analogues[a]

Compound	Conditions	λ_1	λ_2	λ_3	Luminescence	Stokes Shift kJ/mol
$Dipp_3P$	hexanes	205 (11.4)	254(8.7)	326(9.3)	503	129
$Dipp_3P$	ethanol[b]	212	252	325	516	136
$Dipp_3P$	CH_2Cl_2		255(3.95)	327(4.01)	——	——
Ph_3P	cyclohexane			260	445	201
Ph_3P	ethanol			264	500	225
		λ_1	λ_2	λ_3	λ_4	λ_5
$Dipp_3P^{+\bullet}PF_6^-$	CH_2Cl_2	251 (3.99)	281 (3.89) sh	285 (3.91)	296 (3.78)	341 (3.49) sh
		λ_6	λ_7	λ_8	λ_9	
		357 (3.84)	373 (4.04)	456 (3.29) sh	498 (3.31)	
		λ_1		λ_2	λ_3	
$PPh_3^{+\bullet}$	flash photolysis on Vycor	330		345	438	
$PPh_3^{+\bullet}$	50:50 $EtOH/H_2O$[c]	330		320		

[a] Data reported as λ_{max} (nm) with log|ε| in brackets.
[b] Saturated solution, log|ε| not determined.
[c] Joschek H. I.; Grossweiner, L. I. *J. Am. Chem. Soc.* **1966**, *88*, 3261-3268.

Table S3. Table of hfc constants for $[Dipp_3P]^{+\bullet}$ from UB3LYP/6-31G(d) calculations.[1]

Atom/Group	Calc'd Spin Density	Calc'd B3LYP hfc (mT)[2]
P	0.844	**19.2**
C1	-0.146	-0.22
C2	0.12	0.35
C3	-0.054	-0.33
HC3	0.002	**0.03**
C4	0.112	0.14
HC4	-0.005	**-0.08**
C5	-0.043	-0.03
HC5	0.005	**0.29**
C6	0.122	0.57
C7	0.041	0.19
HC7	-0.02	**0.19**
C8	-0.003	-0.01
H_3C8	0.008	**0.07**
C9	0.007	0.09
H_3C9	0.004	**0.03**
C10	0.003	0.04
HC10	-0.008	**0.01**
C11	0.005	0.06
H_3C11	0.001	**0**
C12	0.001	0.01
H_3C12	0.002	**0.19**

[1] Atom numbering scheme is that used in the crystallographic diagram, reproduced below (view is from above the C_3P pyramid).
[2] Boldface numbers indicate isotopes with high abundance (^1H and ^{31}P).

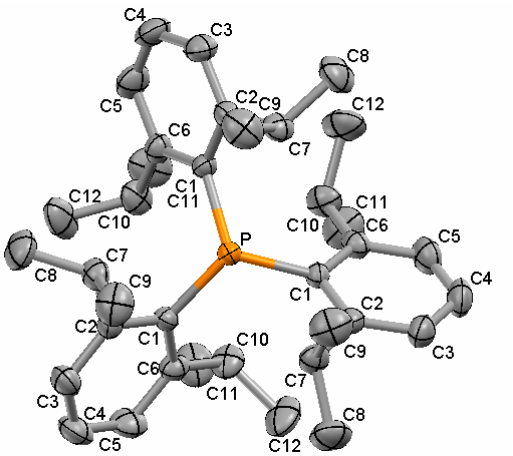

Table S4. Summary of Cyclic Voltammetry Data obtained for oxidation of $Dipp_3P$

Solvent	[M]	Electrode	ν / mV s^{-1}	E°_f / V [a]	ΔE_p /mV	I_p^{ox} /μA	I_p^{red} /μA	$\lvert I_p^{red}/I_p^{ox}\rvert$
DCM [b]	0.558	Pt (1.6 mm)	50	0.08	100	2.11	-2.12	1.00
			100	0.09	103	2.78	-2.79	1.00
			400	0.07	158	4.79	-4.99	1.04
			800	0.08	195	6.25	-6.36	1.02
	0.558	GC (3 mm)	50	0.07	102	7.22	-7.04	0.98
			100	0.07	120	9.90	-9.60	0.97
			200	0.07	144	13.44	-12.60	0.94
			400	0.08	179	16.78	-15.88	0.95
			800	0.08	219	23.30	-21.60	0.93
ACN [b]	0.10	Pt (1.6 mm)	50	0.17	79	0.36	-0.35	0.96
			100	0.18	87	0.49	-0.49	1.00
			200	0.18	76	0.75	-0.73	0.98
			400	0.18	73	1.04	-0.90	0.87
			800	0.18	86	1.31	-1.24	0.95
			1200	0.18	95	1.47	-1.47	1.00
			4000	0.18	138	2.93	-2.89	0.99
	0.10	GC (3 mm)	50	0.17	70	1.28	-1.05	0.82
			100	0.17	68	2.03	-1.65	0.81
			200	0.16	71	2.54	-2.27	0.89
			400	0.16	74	3.56	-2.98	0.84
			800	0.16	83	4.96	-4.30	0.87
	0.10	Pt (11 μm)	20	0.16[c]	71[d]	0.26[e]		
			50	0.17[c]	74[d]	0.25[e]		
			100	0.17[c]	85[d]	0.27 [e]		
		GC (11 μm)	50	0.22[c]	116[d]	0.21 [e]		

[a] E°_f (V vs Fc^+/Fc couple),
[b] Containing 0.1 M $^nBu_4PF_6$ at 295 K.
[c] Half-wave potentials
[d] $|E_{3/4} - E_{1/4}|$
[e] limiting current at microelectrodes in nA.

Table S5. Diffusion Coefficient Values for $Dipp_3P$ obtained by different techniques

RDE [a]	Electrode	D / 10^{-5} cm^2 s^{-1}	RPM
CH_3CN	Pt	1.18	1000
CH_3CN	Pt	1.16	2000
CH_3CN	Pt	1.09	3000
CH_3CN	GC	1.15	2000
CH_3CN	GC	1.14	3000
CH_2Cl_2	GC	1.03	500
CH_2Cl_2	GC	1.05	1000
CH_2Cl_2	GC	1.05	2000
CH_2Cl_2	GC	1.04	3000

CV [b]	Electrode	D / 10^{-5} cm^2 s^{-1}
CH_3CN	Pt	0.82
CH_3CN	GCE	0.87
CH_2Cl_2	Pt	0.93
CH_2Cl_2	GCE	1.19
CH_2Cl_2	Au	0.98

I_{SS} [c]	Electrode	D / 10^{-5} cm^2 s^{-1}	ν/ mV s^{-1}
CH_3CN	Pt (11 μm)	1.22	20
		1.18	50
CH_3CN	GC(11 μm)	1.10	50

[a] RDE = rotating disk electrode 0.1 M $^nBu_4NPF_6$ electrolyte present; D values calculated from Levich equation.[41]

[b] By fitting to the Randles-Sevcik equation 0.1 M $^nBu_4NPF_6$ electrolyte present.[41]

[c] Using limiting current with microelectrodes of indicated diameter, 0.1 M $^nBu_4NPF_6$ electrolyte present, assuming steady-state conditions and equations.

Table S6. Dependence of E°_{f} for the $[Dipp_3P]^{+/0}$ process in CH_2Cl_2 on concentration and $^{n}Bu_4NPF_6$ electrolyte concentration. [a]

$[Bu_4NPF_6]$ / M	R_{mes} / ohm	$[Dipp_3P]$ / mM	E°_{f} / V (vs. Fc^{+}/Fc)
0.511	2150	0.497	0.09
0.051	3160	0.519	0.07
0.511	1950	7.000	0.08
0.051	3160	2.756	0.07

[a] Data obtained at a GC electrode at a scan rate of 100 mV s^{-1}

Table S7. Dependence of cyclic voltammetric data for oxidation of $Dipp_3P$ on concentration.[a]

$[Dipp_3P]$ / mM [b]	ΔEp	Ip / uA
0.497	64	0.825
2.02	71	3.72
4.26	81	9.25
9.23	96	16.5

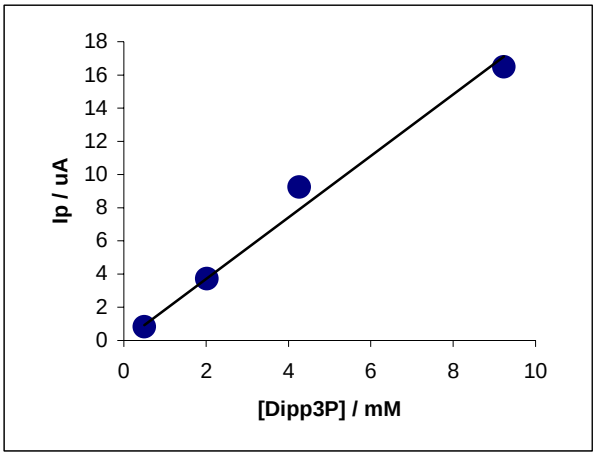

[a] Data obtained at a GC electrode at a scan rate of 95 mVs^{-1}.
[b] In CH_2Cl_2 (0.5 M $^{n}Bu_4NPF_6$).

Figure S1. SS ^{31}P NMR spectrum in a MAS probe of $Dipp_3P$ without spinning and with cross polarization and ^{1}H decoupling. The $\Delta\nu_{1/2}$ is 4.4 kHz.

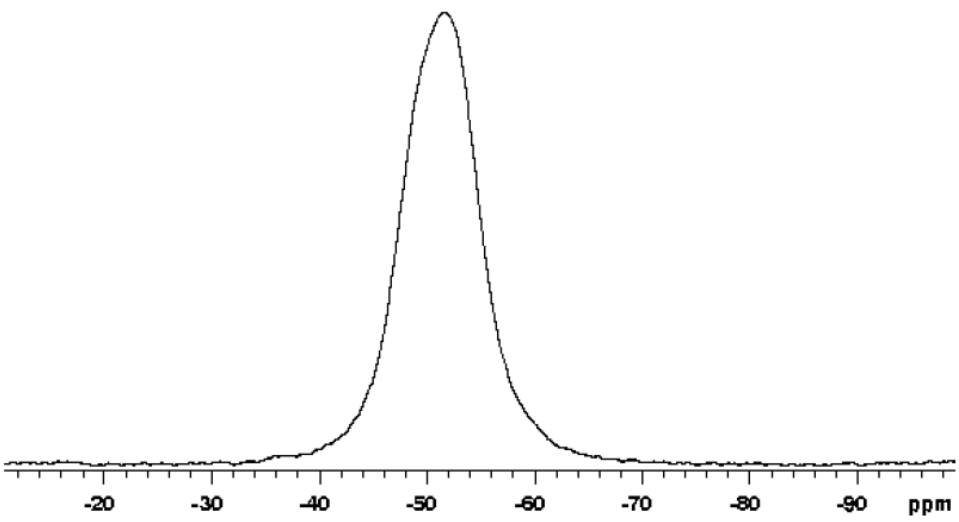

Figure S2 Solution ^{1}H NMR of $Dipp_3P$ in CD_2Cl_2 at -80°C (bottom) and 25°C (top)

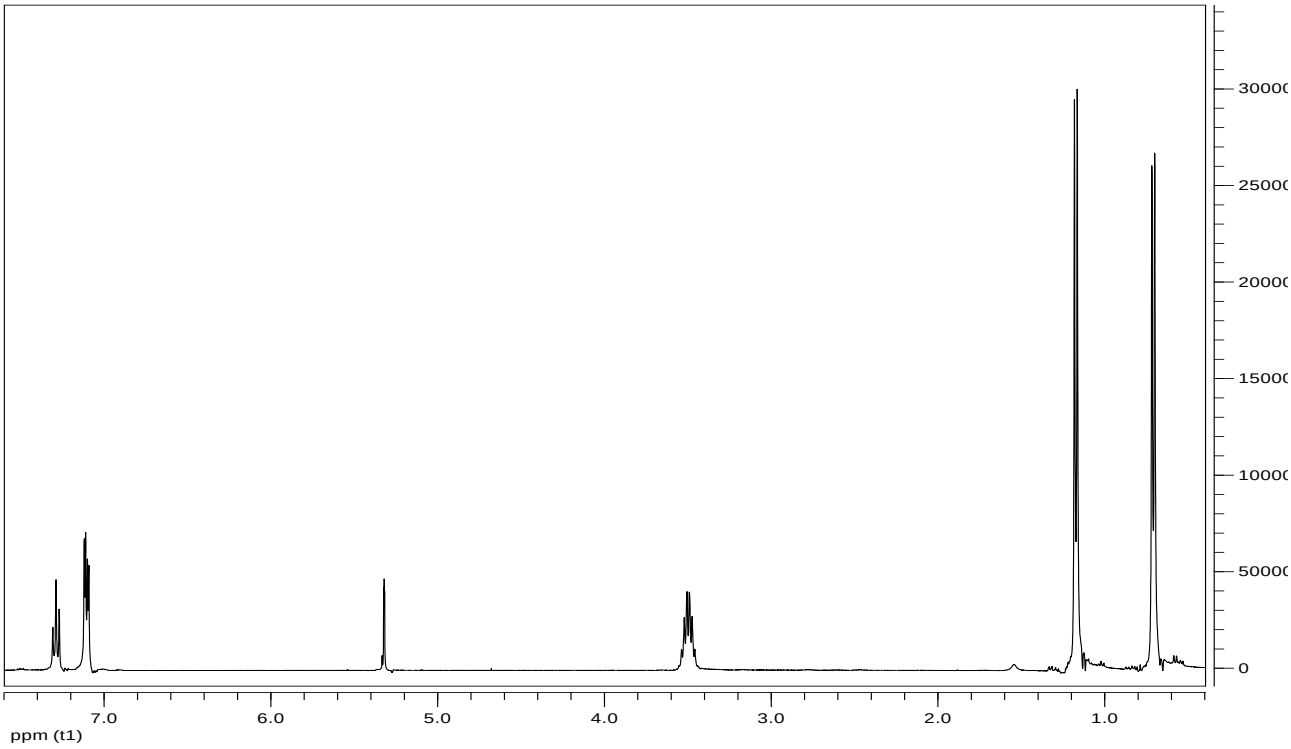

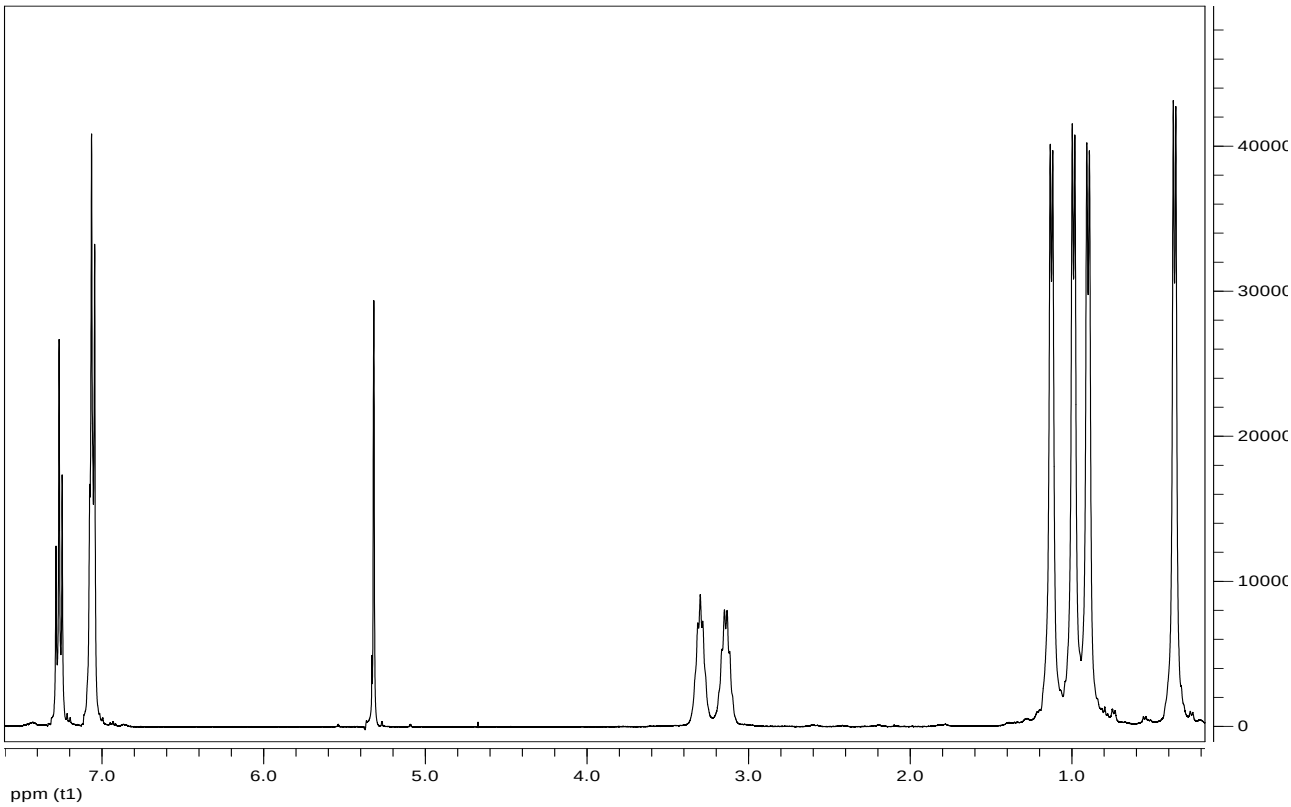

Figure S3 Eyring Plots for the DNMR measurements of $Dipp_3P$ from the $\Delta\nu_{½}$ analysis for ^{13}C and ^{1}H data, respectively, for the isopropyl methyl groups. Experimental data are from the downfield (solid circles) and upfield (open circles) methyl carbon resonances. Lines are linear regression fits.

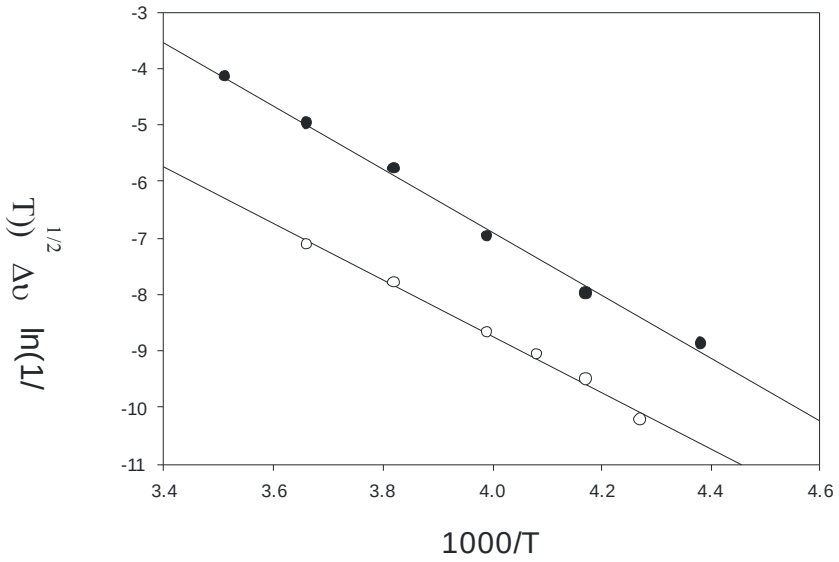

Figure S4 Eyring Plots for the DNMR measurements of $Dipp_3P$ from the LSA analysis for ^{13}C and ^{1}H data, respectively, for the isopropyl methyl groups. Experimental data are from the downfield (solid circles) and upfield (open circles) methyl carbon resonances. Lines are linear regression fits.

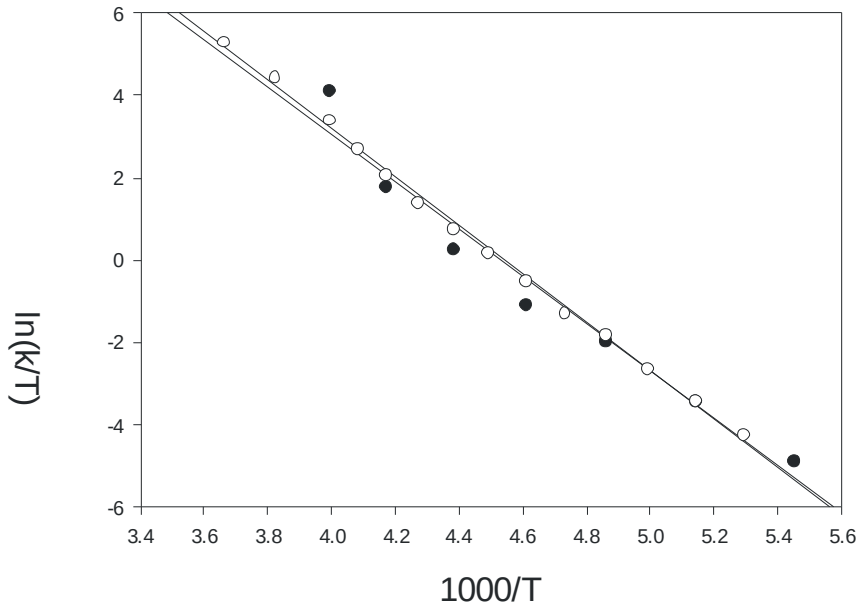

Figure S5 Summary of the Eyring Plots for the DNMR measurements of $Dipp_3P$ for ^{13}C and ^{1}H data, respectively, for the isopropyl methyl groups. Experimental data are all from the downfield methyl carbon resonances, as follows: (solid circles) LSA in ^{13}C; (solid triangles) LSA in ^{1}H; (open circles) $\Delta\nu_{½}$ analysis in ^{13}C; (open triangles) $\Delta\nu_{½}$ analysis in ^{1}H.

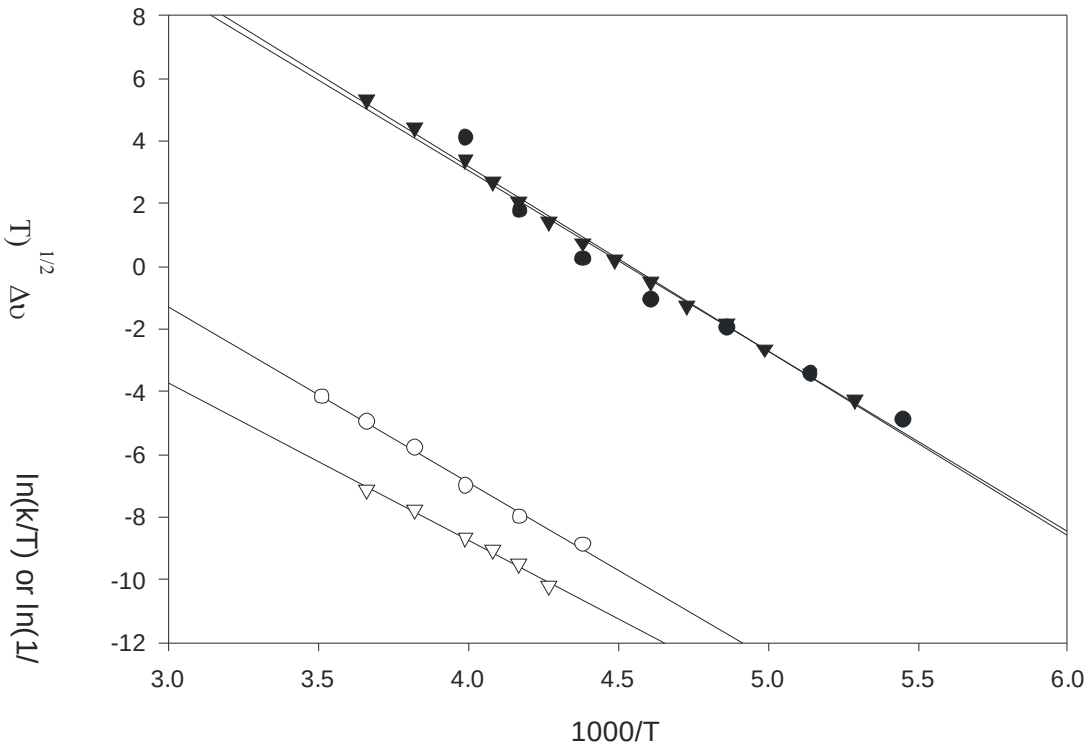

Figure S6 RDE simulated and experimental voltammograms for $Dipp_3P$ (8.85 mM) in CH_2Cl_2 (0.5M $^{n}Bu_4NPF_6$) at a GC electrode. (a) RDE of $Dipp_3P$ before bulk electrolysis and best fit simulation E°_{f} = 0.08 V; α = 0.5; k_s = 0.01 $cm^2\ s^{-1}$; $D_R = D_O = 1.06x10^{-5}$ cm s^{-1}; [$Dipp_3P$] = 8.85 mM; kinetic viscosity of CH_2Cl_2 = 0.0033 $cm^2\ s^{-1}$; electrode radius = 0.15 cm; R_u = 1000 ohm). (b) $[Dipp_3P]^{+\bullet}$ generated in bulk electrolysis, experimental and best fit parameters: R_u = 700 ohm (all other parameters as in a). R_u has decreased from 1000 ohm to 700 ohm because $Dipp_3P^+$ provides additional electrolyte. Potentials vs. $Fc^{+/0}$.

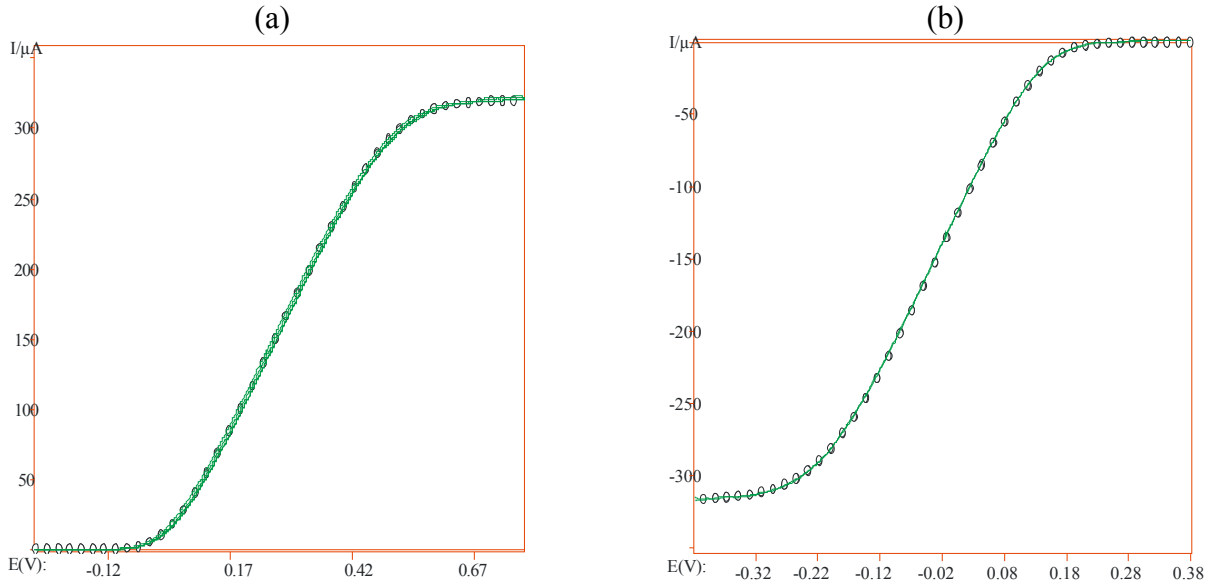

Figure S7 Kohn-Sham total spin density surface plot of $[Dipp_3P]^{+\bullet}$ from a UB3LYP/6-31G(d) calculation. The view is down the 3-fold axis with the P atom in the centre, where most of the spin density is concentrated.

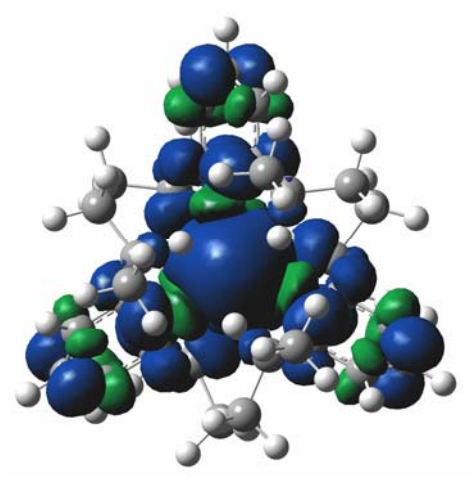

Figure S8 Walsh diagram connecting pyramidal (left) and planar (right) EH_3 frontier orbitals

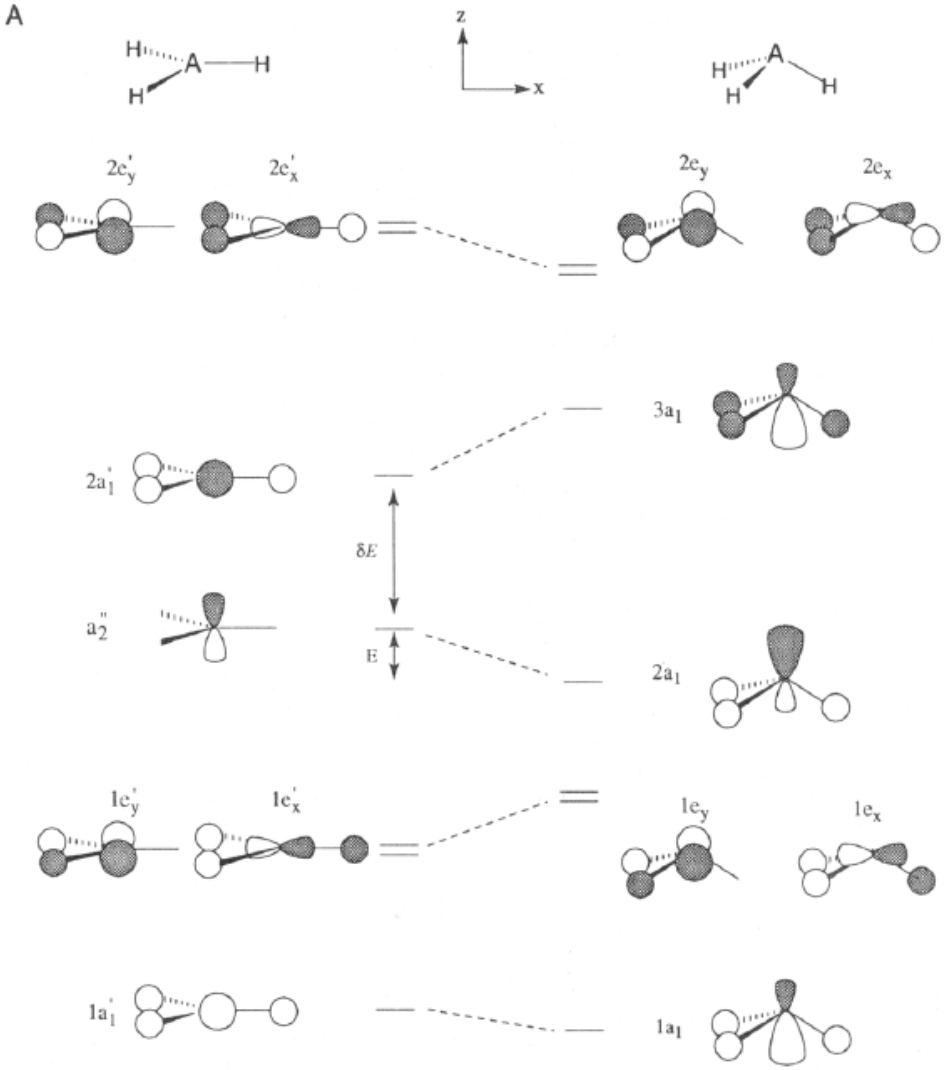

Reproduced from: Gilheany, D. G. *Chem. Rev.* **1994**, *94*, 1339-1374.